ATMOSPHERIC ENTRY SIMULATION CAPABILITIES OF THE IRS PLASMA WIND TUNNEL PWK3 FOR MARS AND VENUS

Georg Herdrich[(1),(2)], Michael Dropmann[(1)], Thomas Marynowski[(1)], Stefan Löhle[(1)], S. Fasoulas[(1)]

(1) Institute of Space Systems, University of Stuttgart,Pfaffenwaldring 31, 70569 Stuttgart, Germany, Email: herdrich@irs.uni-stuttgart.de

(2) CASPER, Baylor University, One Bear Place #97310, Waco, TX 76798-7310, USA

ABSTRACT

An assessment is made for the inductively driven plasma wind tunnel PWK3 with the goal to derive relevant mass specific enthalpies for typical Mars and Venus atmospheric entry missions. For this purpose an integral method has been used which links the plasma power to the radial distribution of total pressure and fully catalytic heat flux in the plasma jet on basis of a relation from Marvin and Pope. Rebuilding the enthalpies with this relation allows for the derivation of a gas specific proportionality factor that enables the derivation of the mass specific enthalpies and the radial profiles for the respective condition are not necessarily required any more. Correspondingly a review of reference CO_2 plasma conditions obtained in past investigations at IRS leads to the identification of an operational envelope in terms of the mass specific enthalpies which are from an energy consideration the prerequisite for the creation of similarities with respect to the real entry maneuvers.

1. INTRODUCTION

Electrodeless inductively heated plasma generators enable basic thermal protection system material tests (e.g. catalysis [1, 2]) and the simulation of atmospheres that contain chemically reactive components such as of Mars or Venus (→ CO_2). The inductively driven generators at IRS have an optimized design where the induction coil is closer to the plasma than it is with other designs [3, 4]. Therefore, the electromagnetic field loss is reduced. The water cooling system surrounds both the coil and the plasma tube.

In the past, several planetary probe missions, soft landing missions and sample return missions such as "Venus Sample Return Mission", "Mars Mini-Probes" Mars Society Balloon Mission or "Mars Sample Return Mission" (MSR)., see the references in [5]. The current reference mission of ESA, ExoMars, has the final goal of a sample return. The sample, however, has to be brought from the Martian surface such that the overall mission has to cope with both an atmospheric entry at Mars and a hyperbolic re-entry for Earth [6]

For such missions both TPS and environment (plasma) during the entry have to be investigated by means of computational and ground facility based simulations. Such ground facilities are the IRS plasma wind tunnels PWK 1-4 reproducing the thermal, aerodynamic and chemical load on the surface of a space vehicle entering an atmosphere. They are operated with different plasma generators. [5, 7]

In addition, plasma wind tunnels can be applied for the development of in-flight instruments e.g. aiming for the assessment of the conditions at the hot structures and / or the plasma conditions experienced by the vehicle during entry [8, 9, 10]. Furthermore, they can be also used to support development activities for instruments to be used for airborne observation campaigns [10]. Reference conditions can be used for validation of numerical tools as well [11]

Non-intrusive measurement techniques like emission spectroscopy, Fabry-Perot interferometry and laser-induced fluorescence are used to investigate the plasma flows [12, 13].

They are applied to determine atomic and molecular density and the velocity distribution in the boundary layer. The laser absorption spectroscopy technique of the Department of Aeronautics and Astronautics (Tokyo University) was used for IRS-PWK3 to determine number densities and translational temperatures e.g. of O_2 [14].

Besides the non-intrusive measurement techniques, mass spectrometry, electrostatic and radiation probes belong to the group of intrusive measurement techniques. Mechanical probes are among the most important instruments for plasma-diagnostic measurements and are often used. Besides the standard sample support system which carries the TPS material sample to be tested, probes for Pitot pressure, Mach number, heat flux, enthalpy and oxygen partial pressure determination are used. Electrostatic probes are used to ascertain the plasma potential, electron density and temperature, energy distribution of the electrons, ion temperature and flow velocity. Radiometric probes are unavoidable when the radiation heat flux can not be neglected compared to the convective part. This is the case when during sample return missions the entry speed into the Earth's atmosphere is especially high or when the atmosphere of another celestial body (that is to be entered) contains strong radiating species, as for example the atmosphere of Titan.

2. EXPERIMENTAL SET-UP

2.1 Facility PWK3

An extensive description of the facility can be found in reference [15].

The PWK3 set-up shown in Fig. 1 consists of the IPG plasma source and the vacuum chamber. The chamber is about 2 m in length and 1.6 m in diameter. Optical accesses enable the investigation of the plasma. A heat exchanger between the chamber and the vacuum system cools down the hot plasma to protect the vacuum system from being damaged. The flat lid of PWK3 (left side chamber) is equipped with the IPG and the external resonant circuit consisting of the capacitors with the connection to the IPG coil. The right side flange of the vacuum chamber is connected to the IRS vacuum pump system simulating pressures at altitudes up to 90 km (Earth entry). Total suction power of the pumps amounts to $6 \cdot 10^3$ m^3/h at atmospheric pressure and reaches about $2.5 \cdot 10^5$ m^3/h at 10 Pa measured at the intake pipe of the system, which has a diameter of 1 m. The base pressure is about 0.5 Pa. The desired tank pressure can be adjusted between the best achievable vacuum and 100 kPa by removing one or more pumps from the circuit and/or mixing additional air into the system close to the pumps.

The external resonant circuit is water cooled. With this, the capacitors, which have a capacity of 6 nF ± 20% each, and the coil are cooled. The resonant circuit depicted in Fig. 2 is built in Meissner type switching using a metal-ceramic triode with an oscillator efficiency of about 75%. Its nominal frequency can be changed by switching the number of capacitors k as well as by the use of coils with different inductivities (variation of coil turns, n).

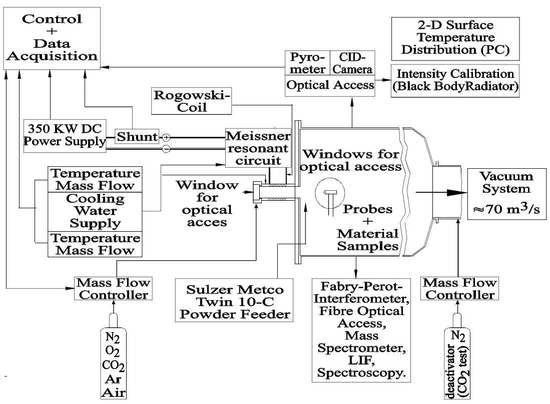

Fig. 1. PWK3 facility set-up.

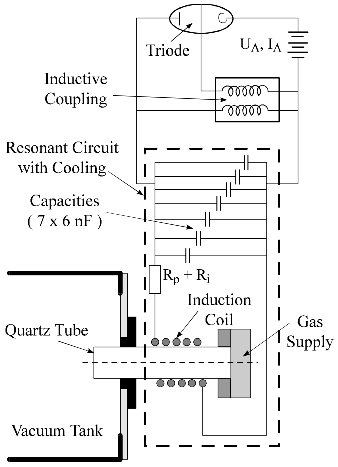

Fig. 2. Scheme of Meissner type resonant circuit.

For the investigations a water cooled 2.5-turn (n = 2.5) and 5.5-turn (n = 5.5) coil, each having a length l of 120 mm, were used. These configurations lead to in¬ductivities L of 0.45 and 1.8 µH, respectively. The whole circuit is connected to a 375 kW power supply. The incoming anode power can be adjusted by the control of the anode (plate) voltage. Correspondingly, the frequency can be approximated by

$$\omega = 2\pi f \approx \frac{1}{\sqrt{LC}} \,. \tag{1}$$

Here, ω is the angular frequency while f is the frequency. The coil inductivity is calculated by

$$L_{coil} = d\,\alpha\left(\frac{d}{l}\right)n^2 \cdot 10^{-7} = g(d,l)n^2 \,. \tag{2}$$

as the well-known relationship for long coils is not applicable anymore [5]. The coil's diameter d has to be inserted in cm leading to the dimension Henry for L. The parameter α, a correction factor, has a magnitude of 6. Introducing the parameter k for the number of capacitors used during operation, the frequency can be determined by

$$f_{n;k} = f(n,k) = f_{1;1}\frac{1}{n\sqrt{k}} \propto \frac{1}{n\sqrt{k}} \,. \tag{3}$$

Usually, there are peripherical inductivities due to the coil's input leads which are not negligible. Therefore, it is useful to use Eq. (3) in empirical form depending on k i.e. for coils with specific n.

With the coils used in this investigation (n = 2.5, n = 5.5), Eqs. (1) and (2) deliver frequencies that are higher than the measured ones. This can be explained by the presence of peripherical inductivities which can be of the same order of magnitude as the coil inductivities:

$$L_{tot} = L_{coil} + L_{Peri} \,. \tag{4}$$

Equations (2) to (4) in combination with the measured frequencies for n = 2.5 and n = 5.5 lead to the frequency range shown in Fig. 3 for PWK3 using the inductively heated plasma generators IPG3, IPG4 and IPG5.

Figure 3 shows the measured frequencies of the facility PWK3 together with the calculated frequencies using equation (1) for different plasmas. Here, Eq. (4) was applied and L_{Peri} was calculated for all measured values. These values depend on the number of capacitors k and on the number of coil turns n. According to Fig. 3, this leads to a frequency range between 0.5 and 1.4 MHz. The usage of just one capacitor together with a 2.5-turn coil ($L_{coil} \approx 0{,}4$ µH) makes a frequency of 1.9 MHz achievable. This value can not be operated permanently due to limitations of the energy supply system and current limiting effects that are ongoing with the capacity reduction. The second coil's (n = 5.5) inductivity is $L_{coil} \approx 1{,}8$ µH. The frequencies shown with filled symbols were measured using a looped conductor connected to an oscilloscope. The open square symbol represents frequencies measured with a modified Pearson current monitor described in [15].

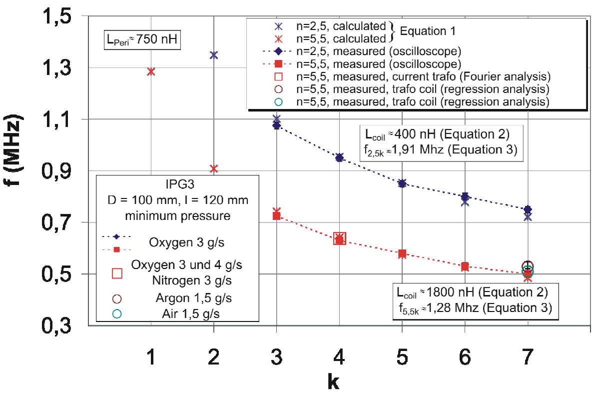

Fig. 3. Measured operational frequencies (n = 2.5, n = 5.5) depending on number of capacitors.

Here, the coil currents for k = 4 were measured with high time resolution for oxygen and nitrogen while varying the mass flow rate and anode power such that frequency spectra could be obtained by Fourrier analysis. For k = 7 a Rogowski coil was used to determine the frequencies for argon and air while varying the plate power. Regression analysis was performed for the data in [15]. With $L_{peri} \approx 0.75$ µH Eqs. (1) to (4) correspond well with the measured frequencies.

Inductively heated plasma generators basically consist of a coil surrounding a plasma container (tube) and capacitors. The alternating current in the coil induces a mostly azimuthal electric field inside the tube. This electric field initiates an electric discharge in the gas that is injected on one side into the tube (see Fig. 4). The produced plasma is expanded into the vacuum chamber. The plasma current amplitude - and thus the Ohmic heating - strongly depend on the electric conductivity of the plasma and the resonant frequency.

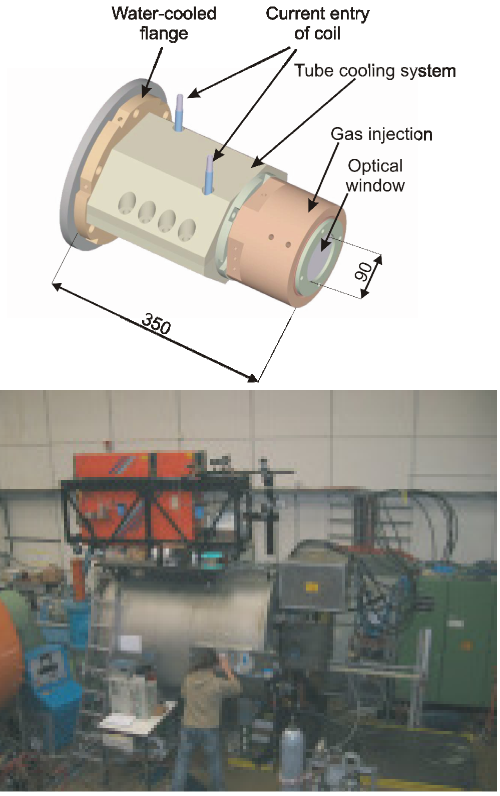

Fig. 4. Inductively heated plasma source IPG3: assembly (upper), photograph of PWK3 (lower).

The principal parts of the plasma generators IPG3 and IPG4 are described here. An axial optical access through the inner injection head enables investigations of the plasma inside the generator. The tube cooling system is transparent. Hence, the position of the "plasma flame" within the tube can be observed with regard to different operating parameters such as chamber pressure, working gas, mass flow and anode power. Additionally, this feature is supported by the axial optical window. The total length of IPG3 is about 0.35 m, its diameter about 0.1 m. The quartz tube contains the generated plasma which leaves the generator through the chamber adapter. The induction coil is connected to the external resonant circuit delivering power and cooling water for the IPGs. Furthermore, both the tube and the coil are surrounded by the tube cooling, which protects the quartz tube from overheating. The water and an additional cage around the generator serve as an rf-radiation protection shield. The length of IPG4 is about 0.4 m (with nozzle). IPG5 is an advanced design where reducing the distance between plasma and coil in turn further reduces the coupling losses [4].

2.2 Measurement Techniques

Cavity Calorimeter

A cavity calorimeter has been developed in order to determine the thermal plasma power in the PWK3 vacuum chamber (Fig. 5). The working principle is easy. The plasma enters the copper cavity, which is shaped like a cone, through a hole. The diameter of the hole is 120 mm, which is roughly 25 % bigger than the usual plasma beams. The distance between the calorimeter and the plasma outlet of the IPG is about 100 mm. This is necessary because smaller distances can result in retroactions that manipulate the discharge behaviour of the IPG [4]. Copper is used due to its very high specific heat conductivity and to its high catalysis. The copper walls are heated up through radiation, convection and recombination. The cavity is equipped with spiral copper tubes that guide the water that cools the copper wall.

With the measured cooling water exit temperature, the cooling water inlet temperature and the cooling water flow rate the plasma power can be determined:

$$P_{cal} = \rho_W c_{p,W} \dot{V}_W \left(T_{out} - T_{in}\right) + \Delta P \ . \tag{5}$$

Here ρ_w is the density of the cooling water, w is the cooling water mass flow rate, $c_{p,w}$ is the heat capacity, Tout is the cooling water outlet temperature and Tin is the cooling water inlet temperature. The parameter ΔP characterizes power losses due to the temperatures and velocities of the hot gas leaving the calorimeter's outlet. The corresponding kinetic power can be estimated using equilibrium models for the enthalpy together with the measured gas temperatures and mass flow rates [15].

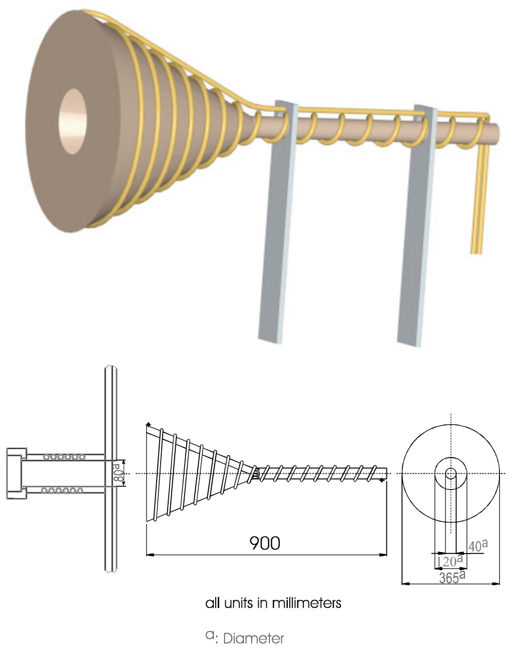

Fig. 5. Calorimeter: 3-dimensional drawing (upper), scheme in PWK3 with dimensions (lower).

A mean specific enthalpy can be calculated:

$$\bar{h} = \frac{P_{cal}}{\dot{m}} = \eta_{tot} \frac{P_A}{\dot{m}} : \tag{6}$$

Steady State Heat Flux / Pitot Pressure Probe

The steady state heat flux is measured on an insert which can easily be changed. Usually, copper inserts are used as a reference. For the steady state case, the flow rate through the insert $\dot{V}$ and the temperature difference of the incoming and outgoing water (T_{out}–T_{in}) are measured, the latter by electrically insulated and shielded resistance thermometers Pt100. The heat flux per unit area is then given by

$$\dot{q} = \frac{c_{p,w} \rho_W \dot{V}_W \left(T_{out} - T_{in}\right)}{A} \tag{6}$$

where $c_{P,w}$ is the heat capacity of water, ρ_w the water density and A the surface area of the probe exposed to the plasma. Figure 6 shows a drawing of the steady state heat flux and Pitot pressure double probe that were used. The heat flux sensor has a diameter of 26.5 mm according to the European standard geometry for heat shield material samples. On the right side the Pitot pressure hole can be seen. For the investigations the same diameter was used. However, a variation of diameter can be performed by exchanging the modular insert for the pressure hole.

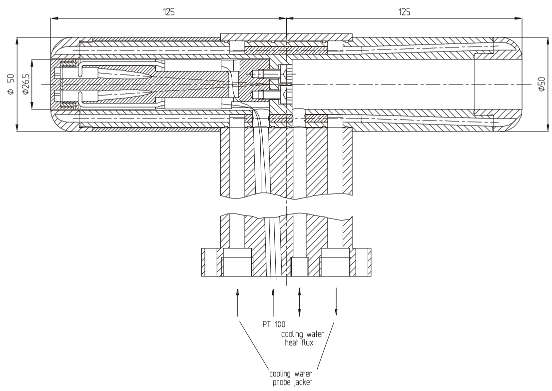

Fig. 6. Scheme of Steady State Heat Flux and Pitot Pressure Double Probe.

The Pitot pressure enables statements on the flow condition, in particular on the Mach number via the Rayleigh-Pitot relation [3].

2.3 Processing of data to obtain mass specific enthalpies

On basis of known fully catalytic heat flux $\dot{q}_{fc}$ and Pitot p_{tot} pressure the semi-empirical equation of Marvin and Pope [16]

$$h = \frac{\dot{q}_{fc}}{K}\left(\frac{p_{tot}}{R_{eff}}\right)^{-0.5} \quad (7)$$

can be used to calculate the mass specific enthalpy. Here, K is a gas specific constant and R_{eff} is an effective nose radius accounting for bluntness of the body contour as e.g. used for atmospheric entry. This effective radius depends on the incident flow condition and for low Mach numbers $R_{eff} \approx 2.3 \cdot R_{probe}$. If in equ. (7) the dependency of both heat flux and pressure on the location was introduced with x as axial distance from the plasma generator outlet and y as radial position of the probe e.g. at a given, then the Integration of the enthalpy over dA with an assumed constant mass flow density yields the plasma power P_{Pl}:

$$P_{Pl} = \sqrt{R_{eff}}\,\frac{2\pi}{K}\frac{\dot{m}}{A}\int_{y=0}^{y=R_{Pl}}\frac{\dot{q}_{fc}(y)}{\sqrt{p_{tot}(y)}}\,y\,dy \quad (8)$$

Equ. (8) can be used to replace K in equ. (7) which leads to:

$$\frac{h(x,y)}{h_{eff}} = \frac{R_{Pl}^2}{2}\frac{\dfrac{\dot{q}_{fc}(x,y)}{\sqrt{p_{tot}(x,y)}}}{\displaystyle\int_{y=0}^{y=R_{Pl}}\frac{\dot{q}_{fc}(y)}{\sqrt{p_{tot}(y)}}\,y\,dy} \quad (9)$$

3. REVIEW OF CO_2 PLASMA CONDITIONS FOR PWK3

An extensive database for experimental conditions of both CO_2 and CO_2 with N_2 has been developed in the past at IRS using the plasma wind tunnel PWK3. A summarizing table of this data base including the associated plasma generator parameters is in the appendix of the paper. In addition, experiments have been conducted with iron oxide powder in order to simulate the dusty atmosphere of Mars. These data are not included in this analysis.

Further measurements in reference [18] imply a significant influence of the catalytic property of the used material as the heat fluxes measured with an iron insert were about 25% larger than the values resulting from the copper base. However, in the analysis showed that this additional heat flux cannot be necessarily traced back to catalysis only and that additional reactions such as e.g. oxidation may took place.

Data obtained by Herdrich are used to calculate the empiric constant K by Marvin and Pope. Having this constant the heat flow of large variety of experiments can be transformed to mass specific enthalpies. Therefore, a comparison of the conditions during Mars and Venus entry and those being generated by the plasma generators at IRS can be conducted.

3.1 Gas specific K from conditions with known enthalpies

Using the cavity calorimeter the plasma power could be measured and hence, knowing the mass flow, the effective specific enthalpy. Additionally the radial heat flux and pressure profiles have been measured at five axial distances to the plasma generator outlet. Thus the specific enthalpies could be calculated using the relation given by Equ. (9). Regarding the determined specific enthalpies, heat fluxes and total pressures on the centreline of the generator the constant K by Marvin and Pope has been determined minimizing the sum of the error squares, when calculating the enthalpy with Equ. (7). The resulting value is shown in Table 1 compared with two values derived from algebraic boundary layer calculations given in Ref. [16]. Additionally a corrected value implying the catalycity of copper oxide is presented. The fully-catalytic heat flux is about 10% higher than the heat flux on copper oxide [17].

K_{CO_2} [kW/(m$^{3/2}$Pa$^{1/2}$MJ)]	Comments
0.28	copper based heat flux
0.31	**factor of 1.1 used to obtain fully-catalytic heat flux, see text**
0.37	Ref. [16] based on Fay-Riddell
0.43	Ref. [16] based on Fay-Riddell

Table 1. Comparison of different values for K

The experimentally determined values for K are about 25% lower than the calculated values given by reference [16] and the references herein. However, these values have been determined using boundary equations based on the derivations of Fay and Riddell. Since this equation takes not well known parameters into account which are even approximated by equilibrium relations (as for example the viscosities at the wall and the boundary layer edge) uncertainties evolve that may explain the resulting differences. This by the way eventually motivated Marvin and Pope to develop a simplified relation as the overall applicability of the aforementioned boundary equations were doubtful. The enthalpies presented throughout this paper have been calculated using the equation by Marvin and Pope using the corrected K being derived by the experimental data by Herdrich.

3.2 Derivation of mass specific enthalpies for further plasma conditions

For the majority of the existing experimental data this K has been used to estimatively provide enthalpies for the displayed conditions (Equ. (7)). The overall data base is then compared with relevant conditions during Mars and Venus entries. The data has been used to characterize the feasible plasma conditions of PWK3. These have been compared with different Mars and Venus trajectories in Fig. 7.

4. OPERATIONAL ENVELOPES OF PWK3 FOR MARS AND VENUS

The data of multiple operating points has been used to find the operational range of PWK3 particularly emphasizing the mass specific enthalpies. Figure 7 shows the results in comparison with those enthalpy and pressure ranges being interesting for entries into the Mars and Venus atmosphere. For Mars the trajectories of the Phoenix and Pathfinder Lander and a typical ballistic trajectory are shown. For Venus the trajectories of the Pioneer Venus Day and Night Probes are shown [21]. Additionally lines of equal height of the Mars and Venus atmosphere are plotted. For Mars the atmosphere is modelled isothermal using density and pressure data obtained by Spirit during descend at an altitude of 20 km. For Venus the obtained atmospheric entry data of the Pioneer Venus Day Probe has been used [21].

In terms of pressure the currently performed operational regime of PWK3 is between 1.3 hPa and 20 hPa. The maximum achieved specific enthalpy is about 63 MJ/kg. By decreasing the mass flow rates even higher specific enthalpies would be possible. The minimum pressure is limited on the one hand by the vacuum pump performance and on the other hand by the plasma generator. However, the limitation of the pressure range so far is of minor importance as e.g. existing similarity models of relevance assume a similarity of mass specific enthalpy while the pressure is linked via the enthalpy to the density during flight. Correspondingly, pursuant to Kolesnikov the similarity of enthalpy conditions during simulations is much more important than the similarity of pressure, as the pressure difference can be compensated by density scaling [19, 20].

The operational range allows simulating the conditions during early Mars entry matching both the enthalpy and pressure conditions. The enthalpy conditions can be reproduced for both Mars and Venus entries at the whole.

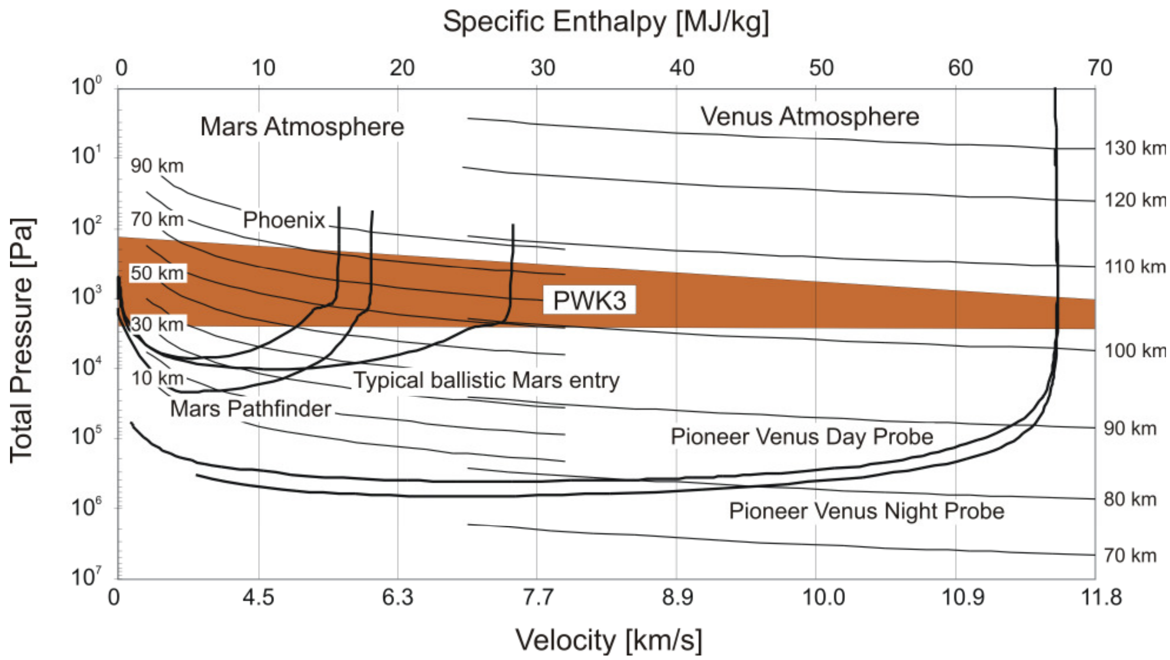

Fig. 7. Operational conditions of PWK3 compared with Mars and Venus entry trajectories

5. SUMMARY

Based on previous measurements of radial total pressure and heat flux profiles of CO_2 plasma in PWK3 the constant K introduced by Marvin and Pope could be determined experimentally. Comparison with values being derived on basis of the Fay-Riddell equation showed deviations of up to 38 %. Different causes of the differences have been discussed. The obtained value for K has been used to determine the specific enthalpies of previously measured CO_2 plasma conditions. Those enthalpies have been compared with conditions during Mars and Venus entry. The comparison revealed that PWK3 is able to provide the enthalpy conditions of the whole for Mars and Venus entry. The limitation of the pressure allows simulating both pressures und specific enthalpies fairly well for

Mars entries. Venus entries are out the pressure range. But pursuant to Kolesnikov the enthalpy conditions are much more important for entry simulations than the pressure as differences in pressure can be compensated by density scaling. Thus as well Venus entry simulations are feasible with PWK3 However the extension of the pressure range will be subject of further research.

6. REFERENCES

1. G. Herdrich, M. Fertig, S. Lein, A. Steinbeck, S. Pidan, Experimental Methodologies and Assessments to derive Catalysis relevant Parameters, Invited Paper AIAA-2010-1247, 48th AIAA Aerospace Sciences Meeting Including the New Horizons Forum and Aerospace Exposition, Orlando, FL, USA, January 2010.

2. G. Herdrich, M. Fertig, D. Petkow, A. Steinbeck, Modeling Approaches for Gas-Surface Interactions, Invited Paper AIAA-2010-1467, 48th AIAA Aerospace Sciences Meeting Including the New Horizons Forum and Aerospace Exposition, Orlando, FL, USA, January 2010.

3. G. Herdrich and D. Petkow, *High Enthalpy, Water-Cooled and Thin-Walled ICP Sources: Characterization and MHD-Optimization*, J. Plasma Physics, Vol. 74, No. 3, pp. 391-429, 2008, doi:10.1017/S0022377807006927.

4. A. Nawaz, G. Herdrich, *Impact of plasma tube wall thickness on power coupling in ICP*, Plasma Sources Sci. Technol. 18 (2009) 045018.

5. G. Herdrich, M. Auweter-Kurtz, P. Endlich, *Mars Entry Simulation using the Inductively Heated Plasma Generator IPG4*, Engineering Note, Journal of Spacecrafts and Rockets Vol. 40, No. 5, pp. 690-694, Sept.-Oct. 2003.

6. Bouilly, JM; Bonnefond, F; Boulier, E; Balemboy, C; Boquet, M; Plaindoux, C; Mignot, Y, Thermal Protection System of the ExoMars Entry Probe, 6th European Workshop on Thermal Protection Systems and Hot Structures, April 2009.

7. M. Auweter-Kurtz, G. Herdrich, S. Laure and H.P. Wagner, *Plasma Source Development for Technical Applications at IRS*, The 4th International Symposium on Applied Plasma Science-ISAPS ’03, Kyoto/Japan 01.-05.09.2003, Advances in Applied Plasma Science, Vol. 4, 2003, S. 157-162, Vacuum, Vol 73/3-4 (2004) pp 309-316.

8. M. Auweter-Kurtz, M. Fertig, G. Herdrich, T. Laux, U. Schöttle, Th. Wegmann, M. Winter, *Entry Experiments at IRS – In-flight Measurement during Atmospheric Entries*, 53rd Int. Astronautical Congress, Houston, TX, USA, Oct. 2002, Space Technology Journal (ST), Vol. 23, Issue 4, pp. 217-234, July 2003, ISSN 0892-9270, R. Monti, Universität Neapel.

9. S. Lein, T. Reimer, K. Stubicar, F. Deuble, M. Auweter-Kurtz, G. Herdrich, M. Winter, *Development of the re-entry spectrometer RESPECT for the ESA capsule EXPERT*, Acta Astronautica, Vol. 64, Issue 4, pp. 395-494, February 2009

10. G. Herdrich, M. Fertig, S. Lein, S. Löhle, A. Preci, A. Steinbeck, R. Wernitz, M. Auweter-Kurtz, Hans-Peter Roeser, *Current Status of Instrumentation Developments at IRS: In-Situ Investigations and Airborne Measurement Campaigns*, Acta Astronautica 66 (2010), pp. 1087–1098.

11. M. Fertig, G. Herdrich, *The Advanced URANUS Navier-Stokes Code for the Simulation of Nonequilibrium Re-entry Flows*, 26th International Space Symposium on Technology and Science, Hamamatsu, Japan, 1.-8. Juni 2008, Selected papers from the 26th International Symposium on Space Technology and Science, Transactions of Japan Society for Aeronautical and Space Sciences, Space Technology Japan, Vol. 7, No. ists26, pp.Pe_15-Pe_24, (2009).

12. S. Löhle, C. Eichhorn, A. Steinbeck, S. Lein, G. Herdrich, H.-P. Röser, M. Auweter-Kurtz, Oxygen plasma flow properties deduced from laser-induced fluorescence and probe measurements, Applied Optics Vol. 47, No.13, pp.1837-1845, 2008.

13. M. Matsui, H. Takayanagi, K. Komurasaki, Y. Arakawa, A. Knapp, G. Herdrich, M. Auweter-Kurtz, *Enthalpy Measurement of Inductively Heated Air Flow*, Journal of Spacecraft and Rockets, Vol. 45, No. 1, pp. 155-157, Jan.-Feb. 2008.

14. M. Matsui, K. Komurasaki, G. Herdrich, and M. Auweter-Kurtz, *Enthalpy Measurement in Inductive Plasma Generator Flow by Laser Absorption Spectroscopy*, AIAA Journal, pp. 2060-2064, Vol. 43, No. 9, Sept. 2005.

15. G. Herdrich, Aufbau, Qualifikation und Charakterisierung einer induktiv beheizten Plasmawindkanalanlage zur Simulation atmosphärischer Eintrittsmanöver, Institut für Raumfahrtsysteme, (in German) Universität Stuttgart, Shaker Verlag GmbH, Aachen, ISBN 3-8322-4338-0, 2005, auch URN: urn:nbn:de:bsz:93-opus-21478, URL: http://elib.uni-stuttgart.de/opus/volltexte/2005/2147/, Dec. 2004.

16. S. Löhle, S. Lein, Ch. Eichhorn, G. Herdrich, M. Winter, Spectroscopic Investigation of an Inductively Heated CO_2 Plasma for Mars entry simulation, submitted to the Journal of Technical Physics, January 2010.

17. A.F. Kolesnikov, M.I. Yakushin, I.S. Pershin, S.A. Vasil'evskii, N.G. Bykova, and A.N. Gordeev, *Comparative Analysis of the Inductive Plasmatrons Capabilites for Thermochemical Simulation at the Earth and Mars Atmospheric Entry Conditions*, XI International Conference on the Methods of Aerophysical Research, 1 - 7 July, 2002. Novosibirsk, Russia.

18. Pia Endlich, *Untersuchungen zur experimentellen Simulation des Eintritts von Raumflugkörpern in die*

Marsatmosphäre, (in German) Dissertation, University of Stuttgart, 2008.
19. Kolesnikov, A.F., *The Concept of the Local Simulation for Stagnation Point Heat Transfer in Hypersonic Flows: Applications and Validation*, AIAA-2000-2515, 21st Advanced Measurement Technology and Ground Testing Conference, Denver, CO, June 2000.
20. Kolesnikov, A.F., Marraffa, L., *An Analysis of Stagnation Point Thermochemical Simulation by Plasmatron for Mars Probe*, Paper AIAA-99-3564, 33rd Thermophysics Conference, USA, Norfolk, Virginia, June/July 1999.
21. A. Seiff, D. B. KIRK, *Structure of the Venus Mesosphere and Lower Thermosphere from Measurements during Entry of the Pioneer Venus Probes*, ICARUS 49, 49-70 (1982)
22. Markus Kuhn, *Vermessung des IPG4 zur Simulation atmosphärischer Manöver im Rahmen von Venus- und Marsmissionen*, (in German), University of Stuttgart, 2001
23. G. Herdrich, M. Auweter-Kurtz, P. Endlich and T. Laux, *Simulation of Atmospheric Entry Manoeuvres using the Inductively Heated Plasma wind Tunnel PWK3*, AIAA-2003-3637
24. P. Endlich, M. Auweter-Kurtz, G. Herdrich, S. Löhle, M. Winter, The inducitvely heated Plasma Wind Tunnel PWK3 as a Means for Emission Experiments to rebuilt radiation Test Cases, ESTEC Plasma Radiation Workshop, Portugal, Lissabon, Oct. 2003.

7. APPENDIX: IRS PWK3 Carbon Dioxide Plasma Condition Data Base

Heat Flux [kW/m²]	Pitot Pressure p_{Pitot} [Pa]	Specific Enthalpy h [MJ/kg]	X Position [mm]	Frequency [MHz]	Number of Capacitors k	Number of coil turns n	Ambient Pressure [Pa]	Mass Flow [g/s]	Anode Voltage [V]	Anode Power [kW]	Comments	Ref.
400	410	17	50	0,64	4	5,5	125	CO_2: 2,2	6600	100	Graphite nozzles used	[22]
310	260	16	60									
230	200	14	70									
200	190	13	80									
230	180	15	90									
160	180	10	100									
420	660	14	50				290					
400	670	13	60									
620	730	20	70									
650	790	20	90									
700	790	21	100									
670	760	21	110									
660	760	21	120									
700	900	20	50				400					
780	960	22	60									
870	1020	23	70									
850	1030	23	80									
850	990	23	90									
850	870	25	100									
810	910	23	110									
800	950	22	120									
1100	1110	28	50				510					
950	1150	24	60									
490	1120	12	70									
940	1070	24	80									
760	1050	20	90									
1440	1900	28	0	0,6	5	5,5	900	CO_2: 3,7 N_2: 0,07	7100	120		[23]
1390	1880	28	10									
1360	1890	27	20									
1320	1920	26	30									
1300	1940	25	40									
1280	1900	25	50									
1240	1890	24	60									
1200	1900	24	70									
1170	1900	23	80									
1140	1900	22	90									
1130	1900	22	100									
700	440	29	100	0,6	5	5,5	190	CO_2: 3,7 N_2: 0,07	7100	120	spectr. data	[24]
1200	1800	24	100				800					

Heat Flux [kW/m²]	Pitot Pressure p_{Pitot} [Pa]	Specific Enthalpy h [MJ/kg]	X Position [mm]	Frequency [MHz]	Number of Capacitors k	Number of coil turns n	Ambient Pressure [Pa]	Mass Flow [g/s]	Anode Voltage [V]	Anode Power [kW]	Comments	Ref.
2570	1230	63	50	0,6	5	5,5	185	CO_2: 3,7 N_2: 0,07	6950	119,5		[18]
2030	960	56	60									
1570	750	49	70									
1410	650	47	80									
1210	540	45	90									
1030	470	41	100									
880	460	35	110									
740	470	29	120									
530	440	22	130									
480	460	19	140									
470	480	18	150									
470	480	19	160									
510	510	20	170									
560	530	21	180									
610	550	22	190									
650	650	22	200									
2520	1480	56	50				500					
2180	1340	51	60									
1860	1260	45	70									
1670	1240	41	80									
1610	1310	38	90									
1690	1400	39	100									
1890	1440	43	110									
1980	1490	44	120									
1890	1450	42	130									
1850	1400	42	140									
1620	1350	38	150									
1370	1400	31	200									
2370	1800	48	50				800					
2080	1740	43	60									
1980	1750	41	70									
1960	1810	40	80									
2000	1850	40	90									
1690	1850	34	100									
1680	1780	34	110									
1650	1760	34	120									
1440	1770	29	130									
1400	1780	28	140									
1360	1750	28	150									
1610	1710	33	200									
2610	1910	51	50				900					
2510	1860	50	60									
2460	1880	49	70									
2410	1920	47	80									
2360	1940	46	90									
2290	1910	45	100									
2230	1890	44	110									
2160	1890	42	120									
2130	1910	42	130									
2070	1900	41	140									
2020	1900	40	150									